AGU PUBLICATIONS

JGR

Journal of Geophysical Research: Oceans

RESEARCH ARTICLE

10.1002/2014JC010688

Filaments on the Western Iberian Margin: A modeling study

Nuno G. F. Cordeiro[1], Rita Nolasco[1], Ana Cordeiro-Pires[1], Eric D. Barton[2], and Jesus Dubert[1]

[1]CESAM and Departamento de Física, Universidade de Aveiro, Campus de Santiago, Aveiro, Portugal, [2]IIM, CSIC, Eduardo Cabello 6, Vigo, Spain

Key Points:
- Filaments anchor to major coastal features over the Western Iberian Margin
- Modeled and satellite filament patterns are comparable
- Wind patterns influence quantity and location of filaments

Correspondence to:
N. G. F. Cordeiro,
ngfc@ua.pt

Citation:
Cordeiro, N. G. F., R. Nolasco, A. Cordeiro-Pires, E. D. Barton, and J. Dubert (2015), Filaments on the Western Iberian Margin: A modeling study, *J. Geophys. Res. Oceans*, *120*, 5400–5416, doi:10.1002/2014JC010688.

Received 30 DEC 2014
Accepted 1 JUL 2015
Accepted article online 4 JUL 2015
Published online 3 AUG 2015

Abstract Coastal upwelling filaments off the Western Iberian Margin, detected in AVHRR satellite imagery and in a realistic ROMS simulation of sea surface temperature, were studied in the upwelling seasons (May–October) of 2001–2010. Sea surface temperature data were retrieved from AVHRR satellite imagery and from a realistic ROMS numerical simulation. The development and variability of the observed filaments were characterized and analyzed during each upwelling season of the 10 year period. Filaments were generally found anchored to the main bathymetric and coastal features but off the more regular northern coast of the Western Iberian Margin their locations were more variable. The results from the modeling analysis reproduced well the general features of filament development. Moreover results of model and observation showed very similar characteristics as those found in the earlier study of Haynes et al. (1993). The model output was used to relate filament patterns, eddy activity, and wind forcing. There was a clear relation between upwelling-favorable wind strength and number and length of filaments, although the relation was weaker in the north of the region. Model filaments were clearly related to eddies only during periods of weak winds. The filament detection method was also applied to a climatologically forced ROMS simulation, which reproduced only gross features of the observed and interannually forced model filament development. This suggests that direct wind forcing and its spatial structure are highly important.

1. Introduction

With the onset of the spring transition in the Western Iberian Margin (WIM), surface stratification develops and strengthens as insolation increases, and the upwelling season starts in response to the northerly winds resulting from the build-up of the Azores high [*Wooster et al*., 1976]. As a consequence, sea level falls close to the coast and an equatorward jet is generated. Associated with the upwelling is a coastal thermal front separating offshore warmer water from nearshore upwelled colder water. The typical temperature gradients across the front are between 0.1 and 0.2°C/km.

This thermal upwelling front becomes subject to frontal instabilities consisting of baroclinic waves of short wavelength (O(20) km) [*Barth*, 1994]. With a succession of upwelling-favorable (northerly) wind events, the thermal front typically moves intermittently offshore until about mid-August, and longer baroclinic frontal instabilities develop [*Narimousa and Maxworthy*, 1989; *Røed and Shi*, 1999] with scales of wavelength about $2\pi \cdot R$ with $R \approx \frac{\sqrt{g'h}}{f}$ being the Rossby deformation radius where g' is reduced gravity, h is surface layer depth, and f is the Coriolis parameter.

In upwelling systems, the instabilities associated with the equatorward jet typically develop into meanders, eddies, and the so-called filaments. The latter are prominent, contorted tongues of upwelled water that extend dozens to hundreds of kilometers offshore and whose width is O(10) km [*Haynes et al*., 1993].

Haynes et al. [1993] considered several filament formation processes along the WIM, originally proposed by *Strub et al*. [1991]. One is filament generation arising from dynamical instabilities on the upwelling-associated equatorward jet. Another is the effect of coastline and continental shelf irregularities (capes, canyons, and promontories) on the separation of alongshore currents and consequently formation of strong offshore fluxes. A third is interaction of preexisting mesoscale field with the upwelling fronts and jets, to generate localized cross-shelf fluxes. In the case of the WIM, the influence of the Iberian Poleward Current and Mediterranean Water vein on the water column can condition the mesoscale field with the presence of meddies and the Mediterranean undercurrent [*Serra et al*., 2010; *Nolasco et al*., 2013]. *Røed and Shi* [1999]

performed numerical simulations for the western Iberian coast with a 1 1/2 layers model, supporting the idea that filament generation is initialized by dynamical instabilities of the equatorward jet that can be intensified or diminished by topographic features.

These formation mechanisms are not mutually exclusive, particularly on the Atlantic coast of the Iberian Peninsula, with its complex bathymetry and coastline (Figure 1). The coastal region contains several canyons (Porto, Aveiro, Nazaré, and Setúbal), a major promontory (Estremadura) and capes. The most important include 90° angled capes (Cape São Vicente, Cape Roca, and Cape Finisterre) and other coastal protuberances such as Cape Sines, Cape Carvoeiro, and Cape Mondego. As was found off Iberia by *Haynes et al*. [1993], filaments are usually anchored to and downstream of the topographic features responsible for the generation of the instability, namely capes and submarine ridges [*Narimousa and Maxworthy*, 1989]. However, in the study of *Røed and Shi* [1999] filaments were found even with straight coastline and bathymetry.

The filaments of cold upwelled water contribute to exchange processes between productive coastal waters and oligotrophic open ocean waters, e.g., the transport of nutrients and chlorophyll to the open ocean [*Cravo et al*., 2010]. Characterizing the frequency, localization, and dimensions of filaments is important for a better knowledge of the exchanges between coast and ocean. This characterization can be based on observational data [*Flament et al*., 1985] or numerical modeling [*Troupin et al*., 2012].

Satellite Sea Surface Temperature (SST) can help identify the surface mesoscale circulation, in which ocean frontal boundaries may be visible [*Bernstein et al*., 1977]. In Eastern Boundary Regions, SST products are commonly used for the identification of upwelling filaments [*Ikeda and Emery*, 1984; *Flament et al*., 1985]. The use of satellite SST products is limited by cloud cover, which interferes with continuous tracking of surface temperature structures. Given the continuity and the degree of realism of surface temperature from numerical modeling, modeled SST can be used to study the filament field along the WIM. To the authors' knowledge, no complete study has been made of filament distribution based on realistic modeling. The present work fills that gap by performing statistical analysis of filaments through modeled and satellite SST fields of the years 2001–2010 in the WIM. The inclusion of the modeling analysis is a major methodological advance from the work of *Haynes et al*. [1993]. Given the advances in observation and modeling of the WIM in the last decades, it is possible to provide more detailed interpretations of the filament behavior than previously, although the emphasis here is on their statistical properties.

The main objectives for this study are to identify the frequency and location of filaments on the WIM, to study the statistics of their occurrence, and to compare the results from analysis of satellite and model-derived SST. Emphasis is placed on determining the preferred formation sites and the temporal evolution of the filaments. Their relation to bathymetric and coastal features, the wind field, and the mesoscale eddy field is investigated.

The data used, the filament detection method, and the wind estimation are described in section 2. Results are presented in section 3, where model and satellite filament distribution are compared. The discussion of the results and the conclusions are developed in section 4.

2. Data and Methods

2.1. Model

The interannual simulation of the years 2001–2010 was run for a high-resolution Regional Oceanic Model System (ROMS-AGRIF) [*Penven et al*., 2006; *Shchepetkin and McWilliams*, 2005]. The model configuration for this study is the same as the one used by *Reboreda et al*. [2014] to study the biogeochemical cycles in the WIM, which in turn is based on the *Nolasco et al*. [2013] climatological configuration. A large domain (not shown here) was first initialized from rest using monthly temperature and salinity climatologies from World Ocean Atlas (WOA09) [*Locarnini et al*., 2010; *Antonov et al*., 2010] as initial condition and at the boundaries. The model was forced with monthly surface fluxes from Comprehensive Ocean-Atmosphere Data Set (COADS) [*da Silva et al*., 1994], similar to the simulation in *Nolasco et al*. [2013]. After reaching equilibrium (5 years), realistic forcing was used at the surface as done in *Reboreda et al*. [2014]. The forcing consisted of the NCEP-2 reanalysis of air-sea fluxes (www.ncep.noaa.gov) and QuikSCAT/ASCAT satellite winds from CERSAT (cersat.ifremer.fr) for the period 2001–2010. QuikSCAT winds were used from January 2001 to February 2009 with 0.5° resolution and ASCAT from March 2009 to December 2010 with 0.25° resolution [*Bentamy*

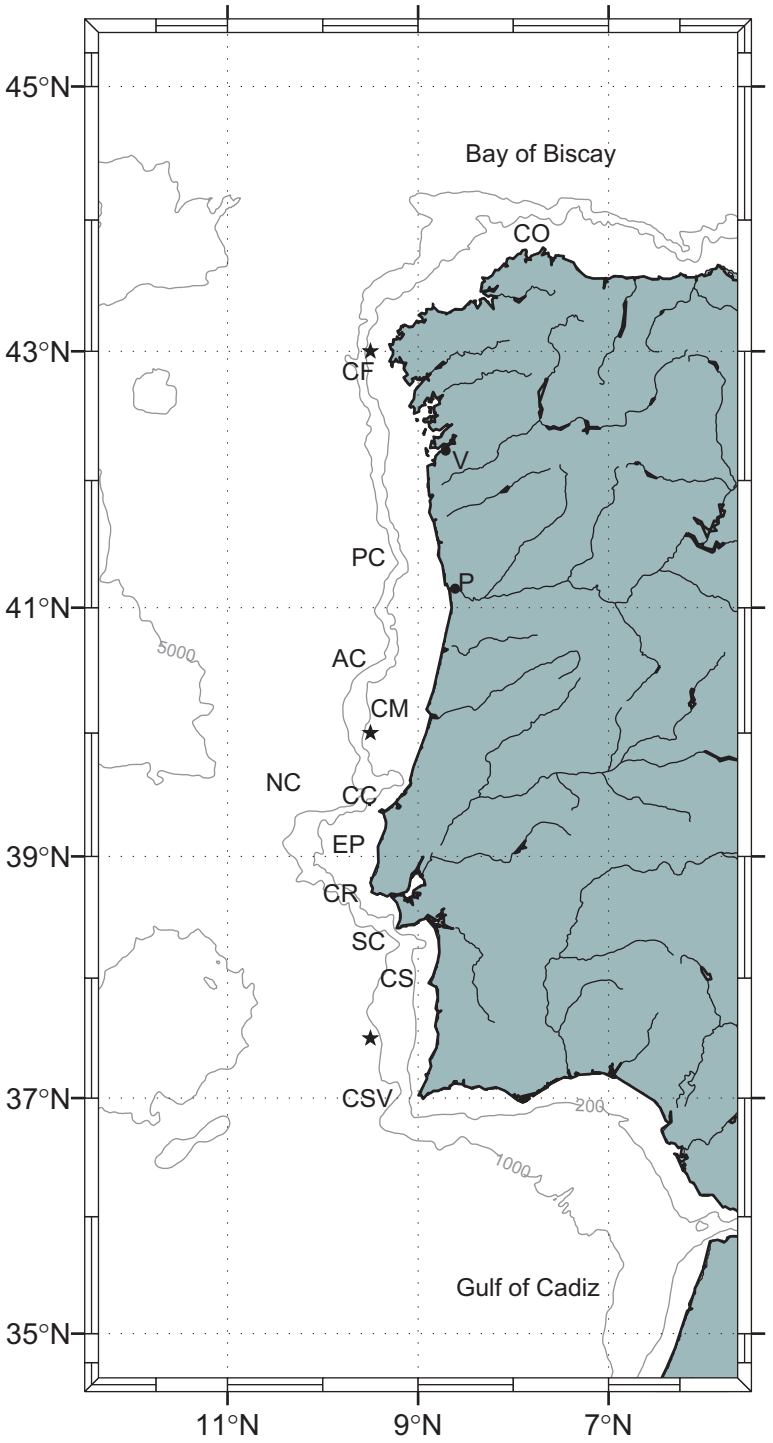

Figure 1. Map of the Western Iberian Margin, bounded to the north by Bay of Biscay and to the south by Gulf of Cádiz. The main topographic features marked on the map are: Cape Ortegal (CO), Cape Finisterre (CF), Porto Canyon (PC), Aveiro Canyon (AC), Cape Mondego (CM), Nazaré Canyon (NC), Cape Carveiro (CC), Estremadura Promontory (EP), Cape Roca (CR), Setubal Canyon (SC), Cape Sines (CS), and Cape São Vicente. Points in land represent the cities of Vigo (V) and Porto (P). The *stars* mark the locations of wind data detailed in section 2.4. Gray contours represent the isobaths 200, 1000, and 5000 m.

and Fillon, 2011]. For the period 2001–2010, the large domain provided boundary and initial conditions for a high-resolution domain (1/27° horizontal resolution and 60 vertical σ-levels, covering the area presented in Figure 1) using an offline nesting procedure. The forcing of the high-resolution domain was the same as

for the large domain. The modeled SST fields in this study were extracted from the daily averaged outputs of the high-resolution domain for the period of May–October of the years 2001–2010.

Validation of the SST obtained by this model configuration was performed with satisfactory results at the monthly scale and the domain scale [*Cordeiro-Pires*, 2013]. Negative bias of SST (i.e., model cooler than observed) was registered on the coastal region, as is common to modeling results of upwelling systems [*Veitch et al*., 2010].

The model configuration is designed to reproduce the mesoscale and is expected to replicate the statistical properties of structure, distribution, and variability of filaments realistically, as was demonstrated by *Marchesiello et al*. [2003] for the California Current. However, it is not expected to reproduce the eddy and filament field in phase with the real one.

2.2. Satellite Data

The filament detection methodology was applied to SST images from satellite infrared products for comparison with model results. Advanced Very High Resolution Radiometer (AVHRR) data of the NOAA were made available by the EUMETSAT Ocean & Sea Ice Satellite Application Facility (http://www.osi-saf.org). The regional SST is available at an approximate resolution of 2 km [*M-F/CMS*, 2009] and was retrieved for the months of May–October of years 2001–2010, for the night satellite pass. The grid was remapped to the same grid as the model.

A visual inspection of the images was performed to exclude any fully obscured by clouds or by physically improbable patterns, such as banding. Images that showed any apparently correct SST field were retained, even if part of the image presented suspect patterns.

2.3. Filament Detection

Pixels with an SST gradient higher than 0.075°C/km were marked on each daily SST image, in order to highlight frontal regions. The gradient threshold of 0.075°C/km was reached empirically in order to be able to detect as much frontal regions as possible. Lower threshold values would show too much noise-generated gradients masking the fronts.

The methodology used for filament cataloging was based on the procedure described by *Haynes et al*. [1993]. Filaments were visually detected, manually marking and recording the longitude and latitude of the extremities. The origin of a filament was determined by the latitude of its coastal extremity, while direction and length were computed using coordinates of both extremities. Only filaments originating along the western coastline, between Cape Finisterre and Cape S*ã*o Vicente, were taken into account.

The origin of a filament was defined as the intersection of the axis of a cold water tongue with the coast. The offshore limit of a filament was defined through the intersection of the northern and southern sides of the previously detected horizontal SST gradient lines. When the orientation of the axis was not clear, some uncertainty occurred in deciding the position of the extremities. This uncertainty was minimized with some practical methods highlighted in Figure 2. (1) Filaments where horizontal SST gradient does not converge to a point were marked on an expected area visible on the temperature field (Figure 2, middle and right, northern filaments). (2) The offshore part of a filament could be visible but the origin would not be detectable due to strong nearshore gradients (Figure 2, middle, northern filament). The origin was marked on the intersection of the approximated bisector between filament sides and the coast. (3) Many of the longer filaments had a curved form (Figure 2, middle, at 39°N) and representing their true form with two points is impossible. In this case, the extremities were marked in such a way as to maintain, as much as possible, the straight line connecting them between the lateral boundaries. This way the direction of the filaments is not biased by the curvature and their length is underestimated with respect to most studies, such as *Haynes et al*. [1993] always considering the offshore extremity as the most distant point from the coast.

This procedure was repeated for the images from May to October in the years 2001–2010. Filament identification was made independently in different images. A total of 5352 filaments in the model and 2115 in the satellite SST images counted for the so-called full set of filaments detected on the Western Iberian Margin. To compare visually the patterns of filaments resulting from the analysis of the model and observed by the satellite, a filter was applied to both full sets of filaments. For each daily image, using the satellite data, cloud coverage percentage was calculated in 50 zonal bands between 36°N and 45°N. The filter consisted

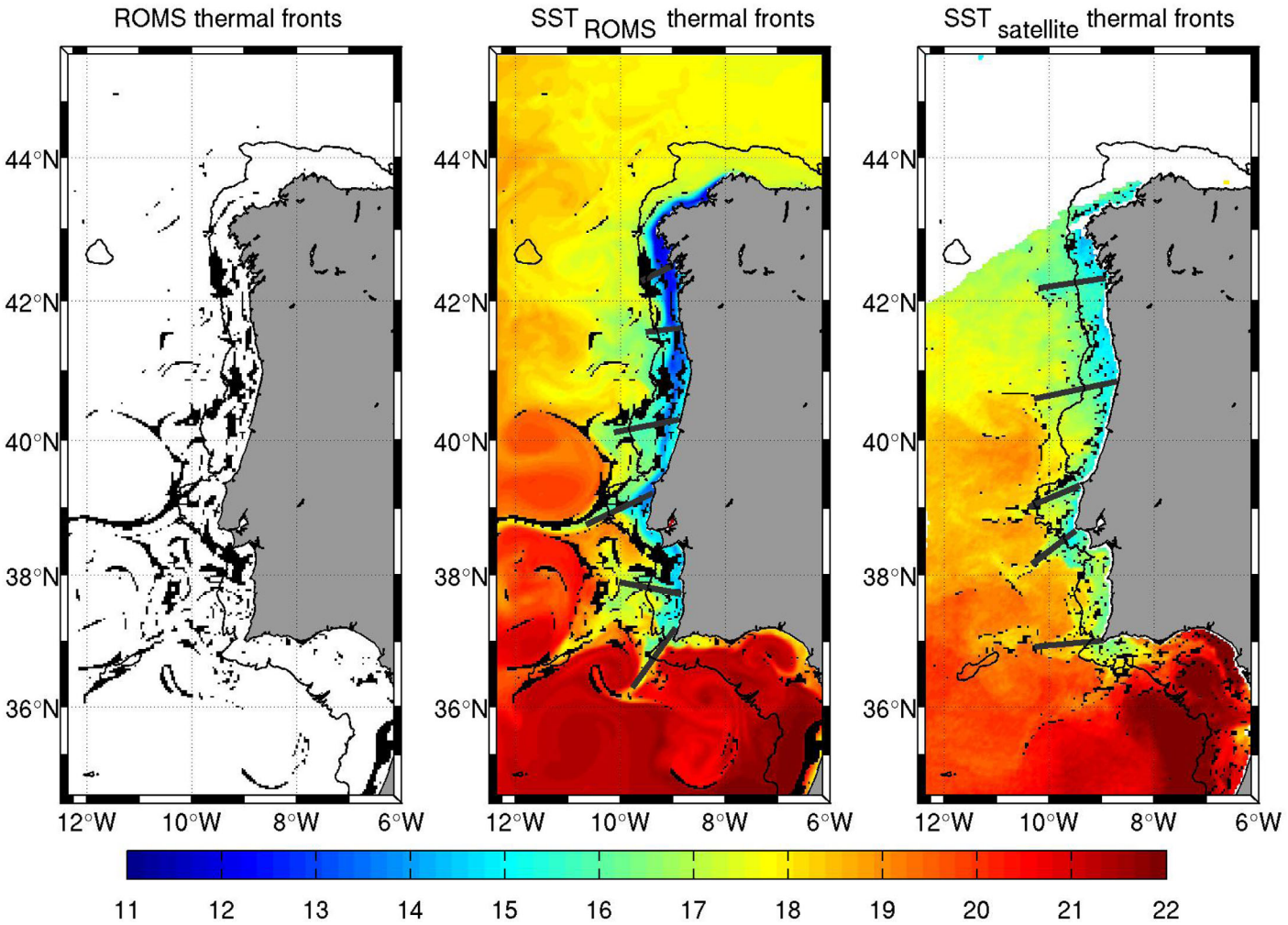

Figure 2. (left and middle) Sea surface images on 17 July 2002 for the ROMS outputs and (right) satellite imagery. Black shading represents horizontal temperature gradients higher than 0.075°C/km. (middle and right) Colored shading is the sea surface temperature and black thick lines extending from the coast are the filaments marked.

in removing filaments observed in zonal bands with cloud coverage higher than 50%. This process was repeated for all images, retaining 1885 model filaments and 1681 satellite filaments, hereafter referred to as the filtered set of filaments. A time versus latitude grid was created to present the temporal development of filament properties in section 3.2. The temporal axis is divided in intervals of 5 days length between days 120 (30 April) and 305 (1 November), and the latitudinal axis is divided in 50 equally spaced intervals between 36°N and 45°N.

2.4. Wind Data

Surface winds, which drive the upwelling, were extracted from QuikSCAT and ASCAT databases (the same as the model winds forcing) for three 0.5° wide square coastal regions along the 9.5°W line, centered at 43°N, 40°N and 37.5°N, see Figure 1.

Figure 3 shows the 10 year mean of the daily meridional wind component on the 40°N square. The study period, in which the filament detection method was applied, is defined between days 121 and 304 (1 May to 31 October), to include the summer upwelling regime. The northerly wind intensity gradually increased until reaching ~6 m/s around day 220 (early August), and decreased afterward until day 295 (22 October) turning southerly from day 290 (17 October). Superimposed on this mean pattern were 5–10 day fluctuations of mesoscale variability of the lower troposphere, generating anomalies such as two periods around

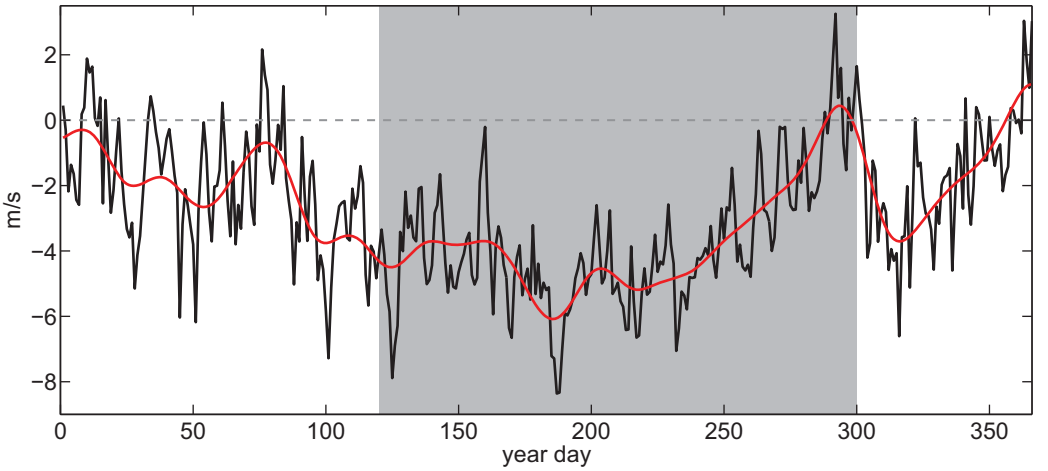

Figure 3. 10 year mean of the daily meridional wind component on the 40°N centered square starred in Figure 1 (black line) and 30 days low-pass filtered (red line). Shaded area indicates the study period (days 121–304).

days 126 (6 May) and 187 (6 July). The zonal wind component (not shown) was mostly directed eastward, decreasing from ∼2 m/s in May to ∼1 m/s in October with few oscillations.

3. Results

3.1. Summer 2002

The distribution of filaments obtained from the satellite products and model output were analyzed for the years 2001–2010; as an example, the particular year of 2002 is examined. In order to perform a comparison between the satellite and the modeled filaments, both are filtered for the effect of clouds, and displayed in Figure 4. The year 2002 was characterized by intense upwelling-favorable winds along the Western Iberian Margin. The upwelling-favorable periods frequently alternated with the passage of atmospheric fronts and cloudiness. The result was the intermittent availability of clear images with large filaments. A low number of filament occurrences were registered in May and June, while during July and August filaments were detected along the entire western coast. From mid-September to late October images were mostly cloud covered, resulting in fewer observed filaments, except late-September north of 42°N. The filament patterns observed in the satellite and modeled images were similar, with two regions of distinct behavior separated

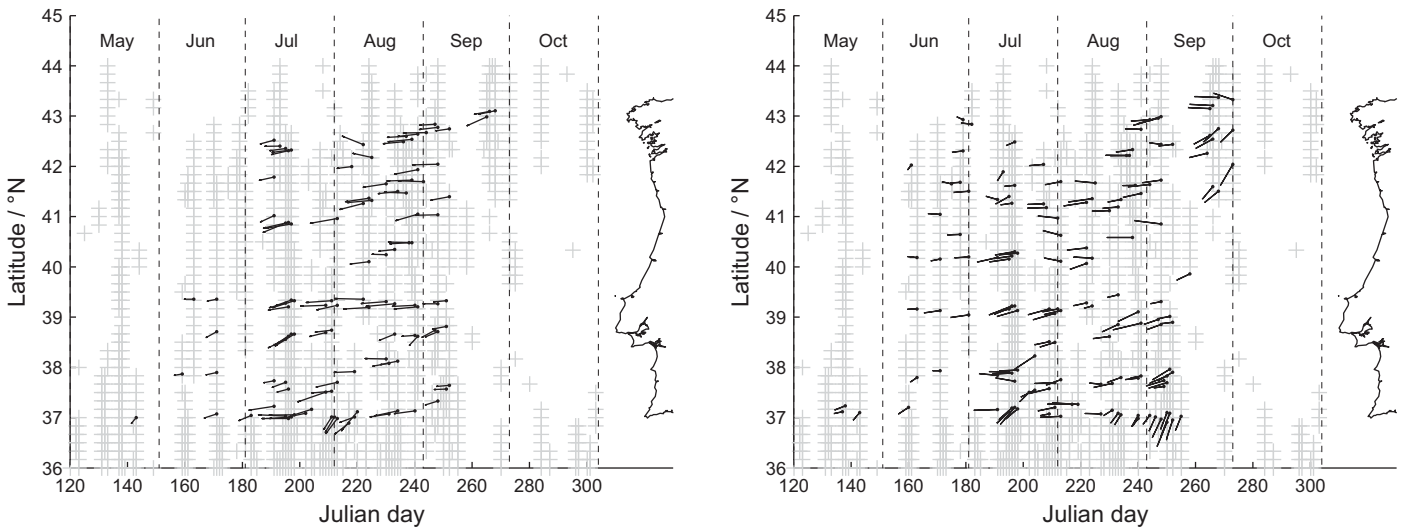

Figure 4. May to October 2002 time series of Filament length and direction (black lines) and latitude of their coastal origin (black dots), observed on zonal stripes with cloud coverage lower than 50% (gray plus signals), from (left) Satellite and (right) Model products.

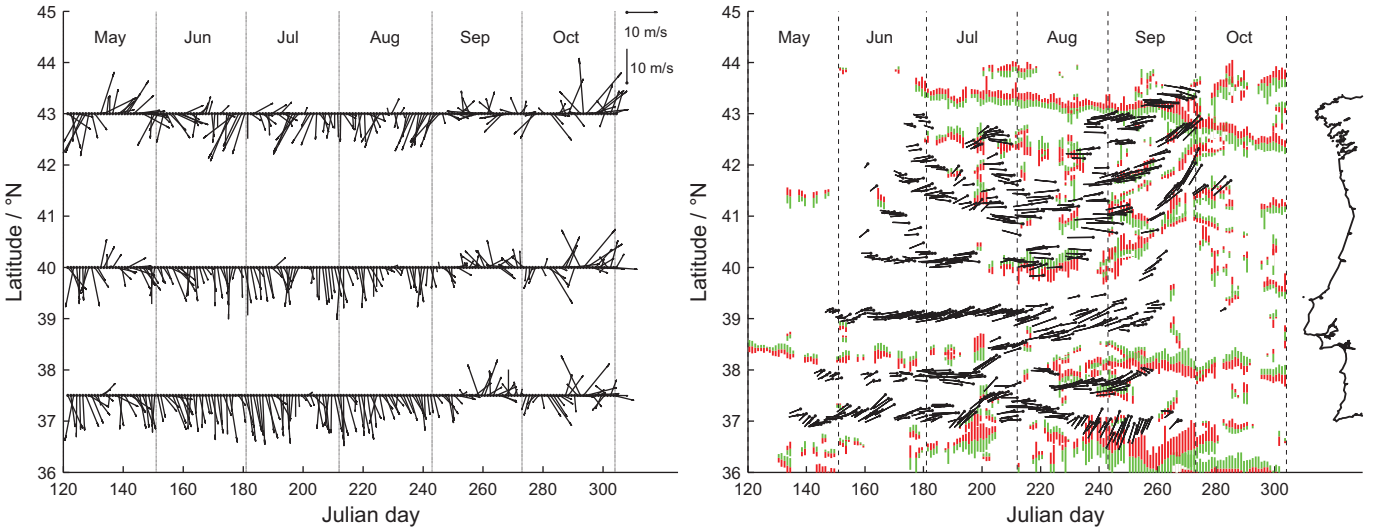

Figure 5. Time series from May to October 2002 of: (left) QuikSCAT wind speed and direction registered in three distinct latitudes at 9.5°W; (right) Filament length and direction (black lines) and latitude of their origin (black dots) on the coast. Green (offshore current) and red (onshore current) colored lines show locations of eddies registered east of 11°W.

by a latitude just north of Cape Carvoeiro (39.3°N). To the south, filaments were observed mostly near the capes and promontories that prevail in the region. To the north, the location of filaments was more variable. These filaments seemed to be shifting southward until early-August and northward afterward.

The most evident differences between modeled and satellite filaments occur in June and July. One difference is the appearance of filaments in the 40°N region in the model field but not in satellite images. Additionally, filaments appeared near both Cape Roca (39°N) and Cape Carvoeiro (39.3°N) in satellite images but not in the model images. In this case, the model filaments in this latitude had a width similar to the length of the Estremadura Promontory between the two capes.

In spite of the differences, the modeling results permit a study of the filament field in the WIM using the full set of model filament occurrences. Results for the year 2002 (Figure 5b) are compared with the temporal evolution of the coastal surface wind at the locations shown by stars in Figure 1 (Figure 5a). To find a connection between filaments and the underlying mesoscale eddies, the distribution of coastal eddies was represented over the filament distribution. The eddy field was obtained by applying an Eddy Detection Algorithm [*Nencioli et al.*, 2010] to the surface current field of the model outputs. Pairs of green and red lines in Figure 5 represent the eddies detected east of 11°W, in which green represents westward currents and red eastward currents.

During June and July, south of 40.5°N, filaments were associated with the main coastal features, around latitudes 37.2°N (Cape São Vicente), 38°N (Cape Sines), 39.2°N (Estremadura Promontory), and 40.2°N (Cape Mondego). North of 40.5°N filaments were initially located at 43°N, 42.5°N, and 42°N, and gradually moved southward until the end of this period, merging into one filament on the 41°N–42°N region as observed in the modeling study of *Røed and Shi* [1999]. The wind was in general northerly, strengthening until late July, frequently interrupted by short periods of relaxation. This upwelling-favorable regime was responsible for the intensification of the surface equatorward flow. Since the northern coast and bathymetry are smoother, filaments initially generated north of 42°N were displaced southward in the sense of the equatorward flow without encountering major obstacles, again as found by *Røed and Shi* [1999]. South of 40.5°N the interaction of the upwelling jet with the principal capes, promontories, and canyons contributed to the characteristic patterns near main bathymetric features.

Although a simple relationship between filament field and mesoscale eddy field is not always noticeable, it can be inferred by following the evolution of filaments and nearby eddies in Figure 5. Generally the eddy field was not related with filament location and orientation in June and July. One exception was found near Cape Sines during a wind relaxation period around day 200 (19 July), in which the filament was located between an anticyclone at 38.5°N and a cyclone at 37.5°N. With the return of northerly winds, filaments

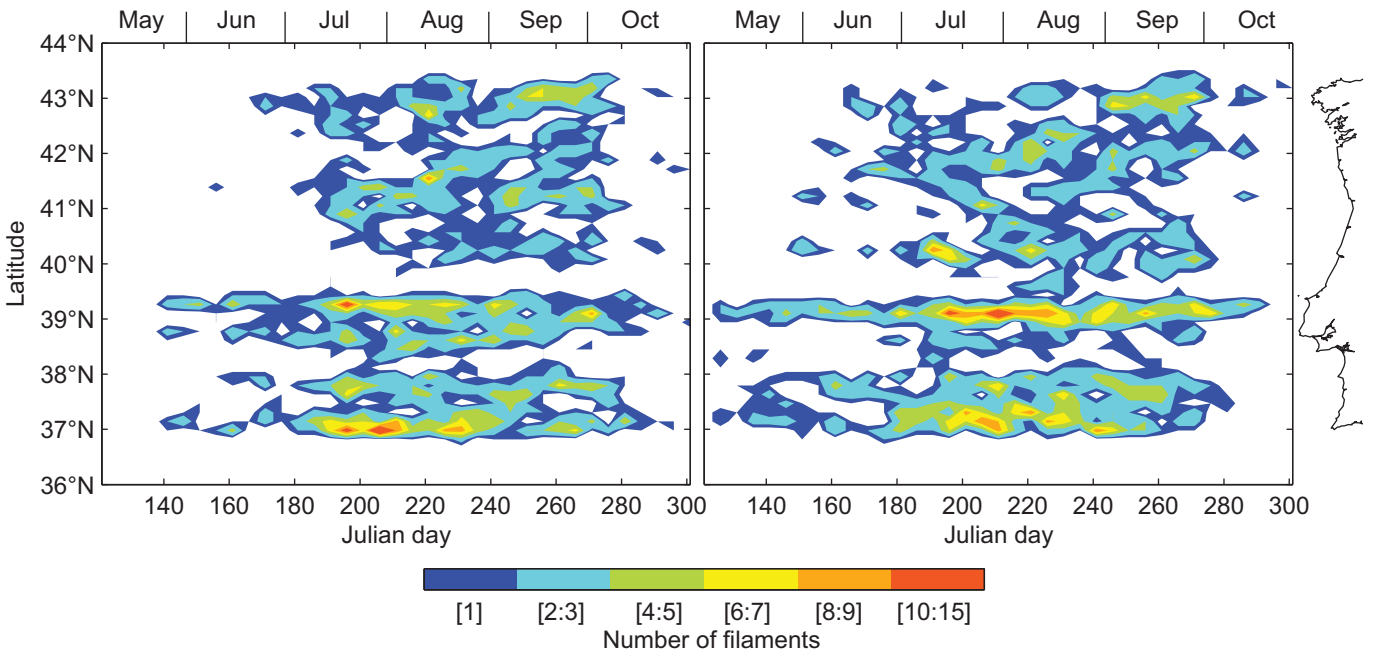

Figure 6. Distribution of the number of filaments observed in zonal stripes with cloud coverage under 50% in the study years, from (left) satellite and (right) model products. The data are divided in 5 days interval and equally spaced latitude intervals between 36°N and 44°N.

previously situated at 37.2°N and 38°N moved northward to 37.5°N and 38.5°N, respectively. In early August, the southern filament gradually returned to its previous position, while the northern one migrated northward to merge with the 39°N filament in the Estremadura Promontory. Also during this relaxation period, the filament located around 40.2°N disappeared. When the upwelling-favorable winds returned, this filament reappeared in association with a local coastal cyclone that developed during the relaxation period.

The August wind regime could be divided in three periods with approximately 10 day duration each. In the first period winds, were mostly strong northerlies that maintained the same filament patterns as in July; in the second, winds were relaxed; and in the third period, strong north-easterlies were found in the northern region while weaker northerlies occurred in the southern region. The relaxation period allowed stratification of the surface layers so that filaments weakened north of 40.5°N. To the south, filaments persisted in the vicinity of the Estremadura Promontory and Cape São Vicente. The formation of an anticyclone at 38°N was accompanied by a filament to the south. During the following upwelling-favorable period, after day 233 (21 of August), a new front was formed between coastal and offshore waters that quickly meandered and, after day 238 (26 August) evolved into two large filaments at 43°N and 41.8°N.

In September the wind weakened and its direction became mostly southerly, contributing to the onset of poleward flow over the slope typical of the time of year. After mid-September, south of 41°N, filaments were no longer observed while those further north were displaced northward under the influence of the poleward flow, until disappearing in early October. As the filaments were displaced in the northward direction, eddies were spun up as a result of instabilities between the warm offshore poleward flow and the cold nearshore equatorward flow. In late August/early September between 36°N and 37°N, a cyclone was situated east of 8.5°W inside the Gulf of Cádiz. Southward flow was generated at Cape São Vicente, coinciding with the southwestward direction of the filaments located at 37°N.

3.2. Annual Integrated Filament Distribution

The temporal and spatial distribution of the 10 year filament field was determined for the defined grid with 5 days spacing on the horizontal axis and 50 equally spaced intervals between 36°N and 44°N on the vertical axis. A comparison between filament distributions of satellite and model data sets is presented using the filaments filtered for clouds (Figure 6). The filament occurrences in the model strongly resembled those in the satellite images and the patterns were similar to a typical year like 2002, as described above (Figure 4). In both data sets, few occurrences were observed in May and June north of 39°N. From July until late

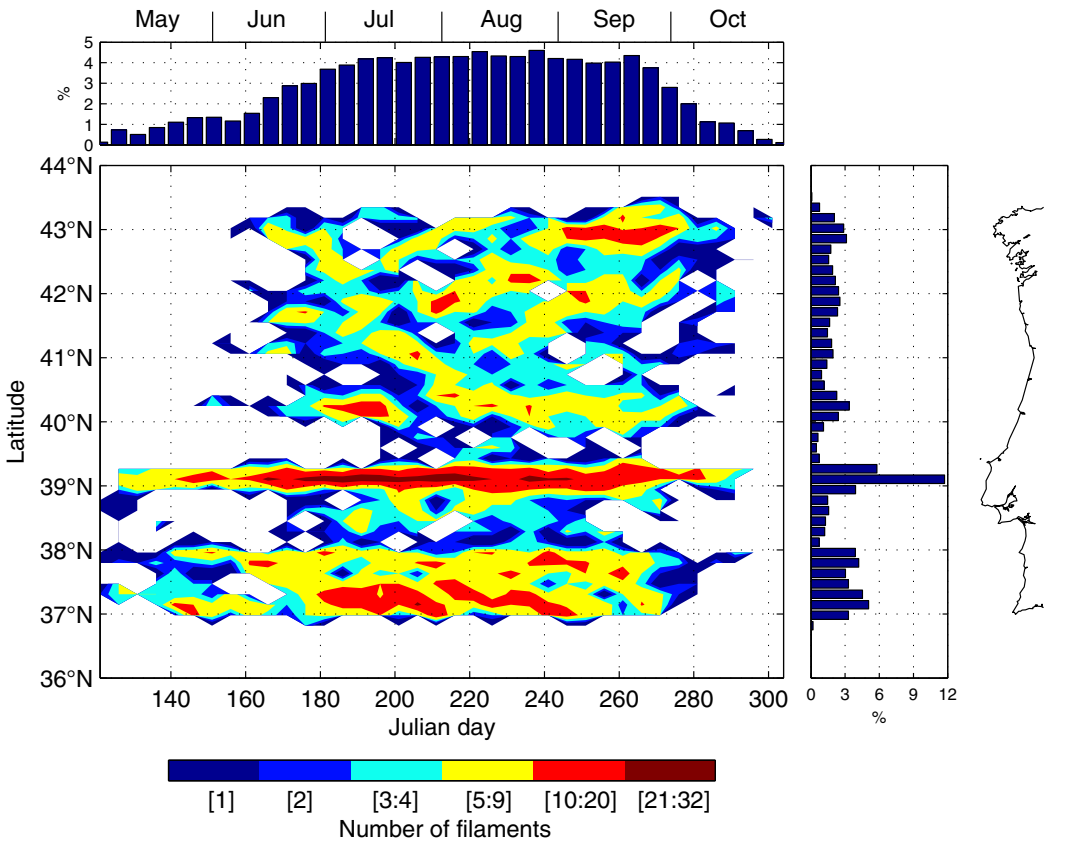

Figure 7. Number of filament observations each 5 days in 50 latitude boxes between 36°N and 44°N, for the 10 years model simulation. Bar graphs represent percentage of filaments integrated for each 5 day interval (top) and for each latitude interval (right).

September, filaments were more common along most of the coastline. Two regions where filaments were not observed by satellite and were seen rarely in the modeled fields were the neighborhoods of 39.7°N, and 38.3°N. Regions with more regular filament occurrences were located near Capes Finisterre, Carvoeiro, Sines, and São Vicente. The differences between model and satellite results documented in the case of the year 2002 extend to the full study period. The model fields presented filaments in the 40°N–40.5°N region all summer, while in the satellite images fewer filaments were observed and only in August and September. The presence of the Cape Sines filament was underestimated in the model, replicating the year 2002 situation, in which a wide filament extended along the Estremadura promontory.

Bearing in mind the performance of the filtered model in comparison with the observations, filament distribution, length, and angle were further analyzed using the full set of filaments from the model. In Figure 7, the distribution of the full set of model filaments is illustrated in the time-latitude grid presented previously. The number of filaments identified in the 10 year simulation for the study period (May–October) was integrated according to time (Figure 7 top) and latitude (Figure 7 right).

Filament occurrences gradually increased until reaching a constant level in early July that lasted until mid-September when occurrences decreased sharply. As expected, the central period accounted for as much as 75% of all filament occurrences, coinciding with the peak of the upwelling season.

The distribution with latitude was dominated by the presence of regions with peaks representing localized high number of occurrences. From north to south, the peaks were located near Cape Finisterre (42.9°N), Vigo (41.9°N), Porto (41°N), Cape Mondego (40.3°N), Estremadura Promontory (39°N), Cape Sines (37.8°N), and Cape São Vicente (37.1°N). The highest peak, at 39°N with almost 12% of occurrences, was associated with wide filaments frequently occupying the Estremadura Promontory, oscillating between Cape Carvoeiro and Cape Roca [*Oliveira et al.*, 2009]. Occurrences of these filaments and the ones near the southern capes were observed throughout most of the upwelling seasons, developing in May and extending to end of

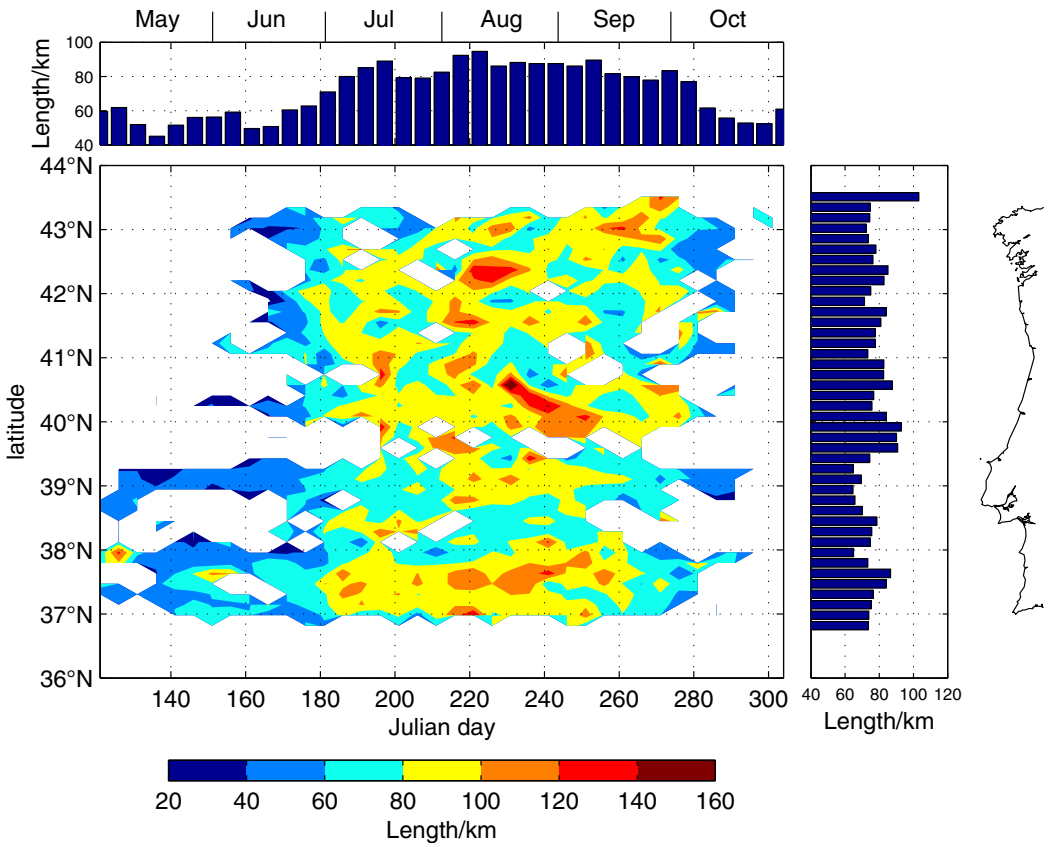

Figure 8. Mean length of filaments (km) observed each 5 days in 50 latitude boxes between 36°N and 44°N, for the 10 years model simulation. Bar graphs represent mean length of filaments integrated for each 5 day interval (top) and for each latitude interval (right).

September with few interruptions. North of the Estremadura Promontory, in most summers filaments did not start to develop until June. The occurrences near Cape Finisterre are concentrated more in September, while near Cape Mondego occurrences remain roughly constant from June to September. The relative maximums near Vigo and Porto are the least localized, indicative of the high mobility of the filament occurrences in the 40.5°N–42.5°N area.

The mean lengths of the filaments observed in the 10 year simulation (Figure 8) increased through the summer, reaching a plateau at roughly the same period as the number of filaments. Integrated according to latitude (Figure 8 right) the filament lengths varied between 70 and 90 km. In regions where filament occurrences were frequent in May and October this value is biased by the shorter filaments, specifically at Estremadura Promontory, Cape Sines and Cape São Vicente. Also, regions with lengthy filaments were not associated with the peaks of high number of filament occurrences. In the Figure 8 (middle) five regions of higher filament lengths are evident, namely between Cape Finisterre and Vigo, between Vigo and Porto, between Aveiro Canyon and Cape Carvoeiro, off Estremadura Promontory and between Cape Sines and Cape São Vicente. The filament number as function of the length was calculated (not shown). The filament length varies between 20 and 200 km, with only a few filaments longer than (1.7%) 150 km. The most frequent length (27%) is between 60 and 80 km.

The angle between the axis of each filament and the east-west direction was determined, in order to evaluate the prevailing orientation of filaments (Figure 9). Positive (negative) angles represent filaments oriented toward the NW (SW) quadrant; thus, an angle of zero represent a filament directed exactly westward.

Three regions of the WIM can be distinguished based on the angle distribution (Figure 9 right): southern, central, and northern. The angle of filaments in the southern region (south of 39.5°N) were mostly negative, directed southwestward, with two peaks immediately south of Cape Roca and Cape São Vicente of approximately −40°. In the central region (between 39.5°N and 43°N), the angles were also negative but closer to

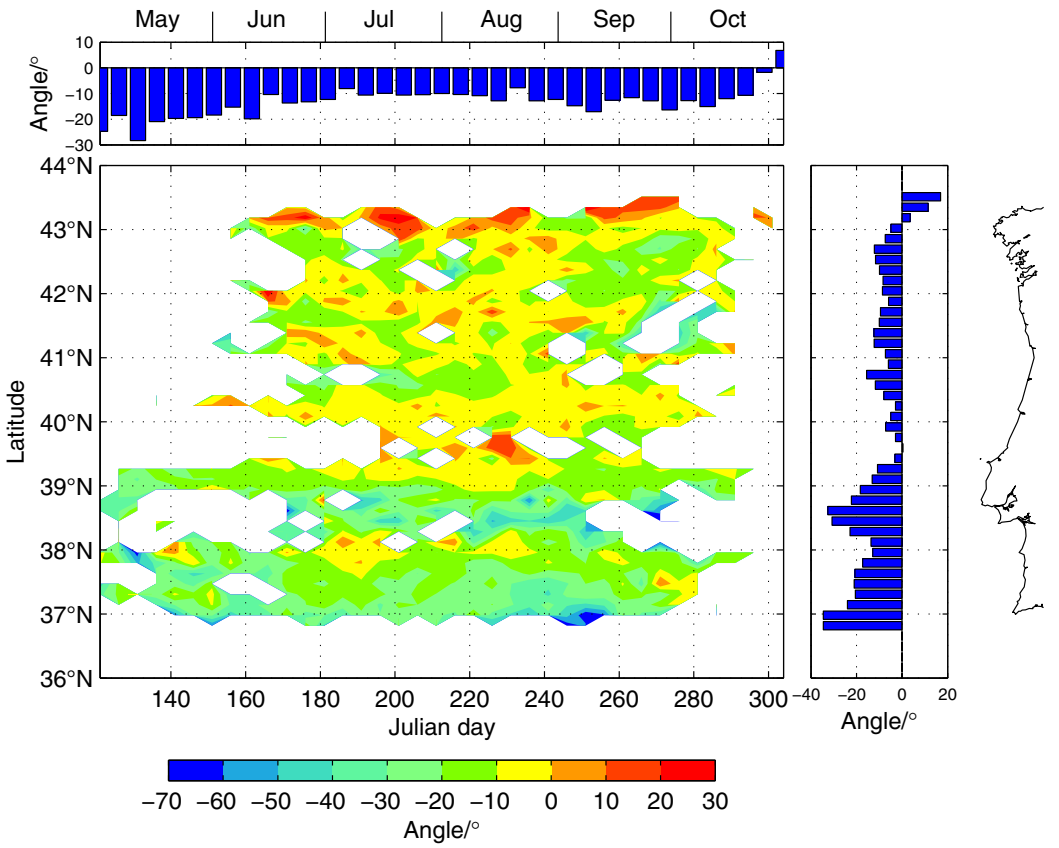

Figure 9. Mean angle filaments make with a westward line at the filament, observed each 5 days in 50 latitude boxes between 36°N and 44°N, for the 10 years model simulation. Bar graphs represent mean sine of the angles integrated for each 5 day interval (top) and for each latitude interval (right). A negative angle indicates southwestward direction and positive is northwestward.

zero, since filaments were mostly directed southwestward and westward, with some directed northwestward. In the northern region (north of 43°N), where the orientation of the coastline shifts to a NE-SW direction, the filaments were mostly directed northwestward.

The angles were generally around −20° (Figure 9 top) evidencing the tendency for southwestward directed filaments. With the exception of the months of May and June, which are dominated by filaments in the south region with few observations, the filaments turned increasingly southward until the beginning of October. After the upwelling period, in late October, filament occurrences were restricted to north of Cape Finisterre, where their direction was mainly northwestward, hence the positive mean angle in the closing days of October.

3.3. Interannual Variability of Filament Distribution

The interannual variability of filament distributions was examined by comparing the monthly number of filaments with the alongshore wind intensity Figure 10. The monthly number of filaments was calculated for two regions with distinct filament patterns, separated at 40°N.

The number of filament occurrences and wind strength was generally lower in the northern region, and filaments were most common in August and September, while in the southern region they were most frequent in July and August. The interannual variability of monthly filaments was generally higher in the northern region than in the southern one.

In the northern region, some years did not present filaments in May and the others were weak. For June and October, the same occurred but with more number of filaments. For the remaining months, a high number of filaments was present in 2002 (June and September), 2009 (August and September), 2010 (July and August), 2006 (August), 2001 (July). Fewer filaments were observed in 2009 (July), 2007 (July), 2008 (September), and 2004 (August).

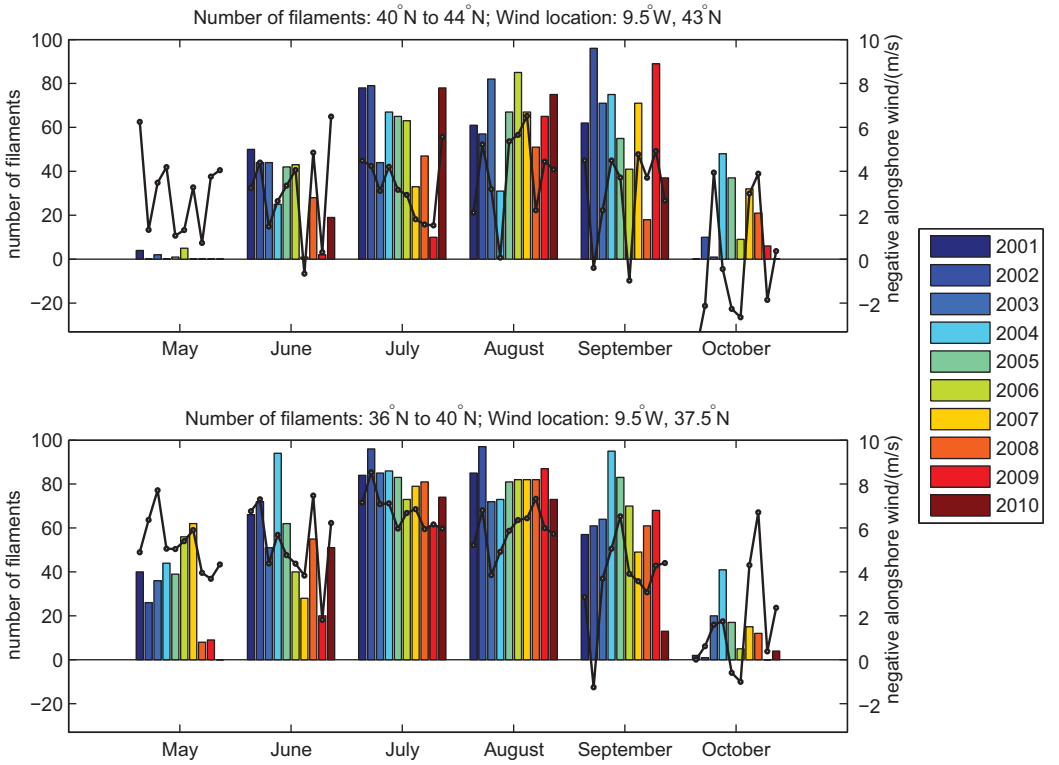

Figure 10. Monthly and yearly integrated number of filaments (bar graphs) and negative of the monthly means of alongshore winds (*circles*) on the northern region (top) and the southern region (bottom). Positive (negative) values mean northerly (southerly) winds.

In the southern region, some years did not present filaments in May and October while others presented few filaments. In May, number of filaments was considerably higher than in the northern region. In June and September, filaments were observed for all years, although with relatively high interannual variability, e.g., in 2004 filament numbers were on the order of the top monthly occurrences (>80 filaments/month), while September 2010 and June 2009 presented <20 filaments/month. In July and August, filament occurrences were higher than 60 filaments/month, with 2002 presenting the greatest number of filaments in both months. The interannual variability of these months was significantly lower than any other in the southern region and than all months on the northern region.

In May and October less relationship between filament number and alongshore wind was found, possibly because the number of occurrences was low. In the months with most occurrences (June, July, August, and September), the number of filaments followed trends similar to the intensity of alongshore winds. With stronger monthly northerly winds, more filaments were observed, except in September 2002, which had numerous filaments despite southerly winds. This was the only month when filament number was relatively high and mean monthly winds were southerly.

The explanation of this anomalous behavior in September 2002 is evident in Figure 5. Strong northerly wind from late August to 10 September generated several persistent filaments along the WIM. After that date, wind was variable in the northern region, and southerly in the southern region. Consequently, filaments maintained their identity throughout the northern region, but disappeared in the second half of September in the southern region.

3.4. Filament Distribution on a Climatological Simulation

In order to evaluate the dependence of the wind variability on the filament field, the filament detection method was also applied to the results of a climatological model simulation [*Nolasco et al.*, 2013]. The surface fluxes were obtained from the COADS which consisted in monthly climatological wind and heat fluxes without interannual variability, run through 9 consecutive years. For filament detection, images of 3 day averages of SST were produced from the years 6–9 of the simulation.

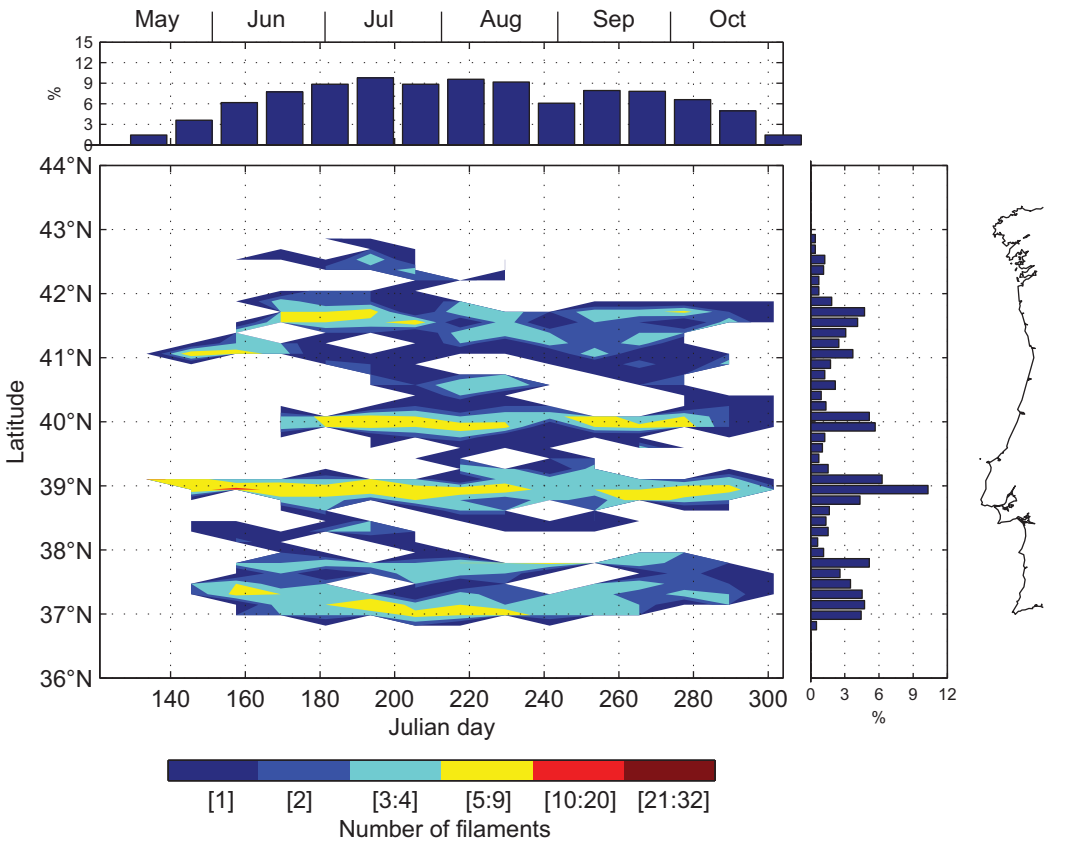

Figure 11. Number of filament observations each 12 days in 50 latitude boxes between 36°N and 44°N, for 4 years of the climatological simulation. Bar graphs represent percentage of filaments integrated for each 12 day interval (top) and for each latitude interval (right).

The temporal and spatial distribution of the 4 year filament field was analyzed, as in Figure 7, on a grid spaced at 12 days on the horizontal axis and in 50 equal intervals between 36°N and 44°N on the vertical axis. The distribution of the filaments is illustrated in this time-latitude grid (Figure 11) with temporal integration (Figure 11, top) and latitudinal integration (Figure 11 right). The evolution of filament number through the climatological summer was characterized by an increase of occurrences in May and June, a maximum in July, a high number in August, and decreasing numbers in September and October.

The main regions for filament occurrences were located between Vigo and Porto, near Cape Mondego, off the Estremadura Promontory region near Cape Sines, and off Cape São Vicente. These regions presented filaments during most of the May–October period. North of Vigo some filaments were registered in June and July but were not present after August. By direct inspection of the SST field (not shown) and from Figure 11, filaments north of Cape Mondego were displaced southward between June and August, as seen in the slope of the distribution of number of filaments.

4. Discussion and Conclusions

The field of upwelling filaments generated in a numerical model of the WIM was analyzed and compared to a database of satellite images for the common period 2001–2010, using methods similar to the *Haynes et al.* [1993] study of the period 1982–1990. The results from both periods and studies are similar in that filament generation over the WIM is associated with periods of fully developed upwelling, occurring every summer mainly during July and August. Filaments are generated along most of the WIM with different patterns in distinct regions. In the region between Nazaré Canyon (40°N) and Bay of Biscay, filaments are concentrated in the neighborhood of Cape Finisterre (43°N), Vigo (42°N), Porto (41°N), and Cape Mondego (40.3°N). The

filaments associated with Cape Finisterre and Cape Mondego frequently remain anchored to these capes. The region between these capes has a relatively straight bathymetry, although several submarine canyons exist (Porto and Aveiro canyons, see Figure 1). In this region, there is evidence [*Peliz et al*., 2002] that the poleward flow offshore (and its mesoscale features) interacts with equatorward flow on the shelf, generating horizontal shears, and hence instabilities, evolving into filaments. The occurrences off Vigo and Porto are related with filaments that move appreciably alongshore around those latitudes. In general these filaments are displaced southward during June and July and northward in August, September, and October. The southward displacement might be related to the general strengthening of the equatorward flow at the beginning of the upwelling season. In September and October, filaments are usually advected northward by the presence of the Iberian Poleward Current until the coastal cold SST signature of upwelling is overrun by the warmer oceanic surface water.

In the region between 39.5°N and 40°N, few filaments were found in either satellite or model fields. This lack of filament generation might be related to a predominantly anticyclonic circulation in the region north of the Estremadura Promontory, associated with the separation of the Mediterranean Water vein at depth from the Estremadura Promontory [*Nolasco et al*., 2013].

Further south on the same promontory both Cape Carvoeiro and Cape Roca give rise to separate filaments that frequently merge together. This situation occurs more commonly in the model, where it results in underestimation of the Cape Roca filament occurrences (Figure 6). Near Cape Roca, filaments with strong southward component can be a consequence of overshooting of the equatorward upwelling jet, as suggested by *Relvas and Barton* [2005], for the similar case of Cape São Vicente. This occurrence frequently shelters the region south of it, such as in Monterey Bay in the California Current [*Graham et al*., 1992]. This is also observed south of the Estremadura Promontory [*Moita et al*., 2003], at the Setubal canyon region, where filaments are rare.

From Cape Sines to Cape São Vicente, a high number of filaments is observed with most occurrences at or near these capes. Filaments are mostly located downstream of Cape Sines and upstream of Cape São Vicente, but have a tendency to migrate and merge between both locations. These filaments usually have a SW direction and, in the case of Cape São Vicente, filaments can have a stronger southward component associated with periods of cyclonic circulation generated in the southern margin near the cape.

Studies in other Eastern Boundary regions have also concluded that the most extended and predominant filaments are associated with the major capes and ridges. South of Iberia in the Canary Upwelling System major filaments are frequently associated with the Cape Ghir plateau [*Troupin et al*., 2012]. Further south still at 20°N filaments were identified near Cape Blanc, where *Meunier et al*. [2012] report on the relation between filament structure, eddies, and bathymetry. *Kostianoy and Zatsepin* [1996] reported on filaments off both NW Africa and in the SW African region in the Benguela Upwelling System. In the latter system, no relation between filament location and coastal features was observed. In the California Current System, where upwelling filaments were first identified [*Breaker and Gilliland*, 1981], between Cape Blanco and Point Conception, upwelling filaments, of lengths up to 300 km, are associated with the main coastal features [*Flament et al*., 1985; *Strub et al*., 1991].

In the Northeastern Atlantic upwelling system between 15° and 20°N the upwelling season occurs in winter/spring while north of 20°N it occurs progressively later with increasing latitude, occurring in summer in the WIM. The temporal evolution of the filament field through the May to October period starts with the development of small structures mainly anchored to the capes south of 40°N. As the upwelling season progresses, filaments grow and develop in most of the preferred sites named above. At the end of the upwelling season, the number of filaments decreases as the upwelling-favorable winds decrease and the upwelling jet slows. Filaments are rarely observed along the WIM after the onset of northward surface flow in the Iberian Poleward Current over the slope region [*Relvas et al*., 2007].

In *Haynes et al*. [1993], filaments had systematically greater lengths and were found in narrower location ranges than in this study. These differences are partly related to the subjectivity inherent in this kind of studies, and to small differences in methodology. While *Haynes et al*. [1993] based their analysis on individually contrast-enhanced, gray-scale images supplied as prints by the UK Dundee Remote Sensing service, the present study used standard downloaded color-coded image products from EUMETSAT Ocean & Sea Ice

Satellite Application Facility. The different definition of the filament termination used in this study (see section 2.3) resulted in underestimation of about 40 km in the mean filament length (from 120 km in *Haynes et al*. [1993] to 80 km here). This underestimation occurs, since in this study, the offshore filament termination was marked as the point where the northern and southern boundaries of the filament converge, even if it extends visually further from this point. On the other hand, marking pixels with high SST gradients allowed more precise positioning of the filament origin at the coast. Despite the above apparent differences in results between the two studies, the main filament locations reported here for 2001–2010 and found by *Haynes et al*. [1993] for 1982–1990 are remarkably similar. Nevertheless, while those authors found the maximum number and length of filaments occurred in September, here it is found that the months of July–September all have equally high occurrence and maximal length.

In the WIM northerly winds largely control the upwelling intensity [*Fiúza et al*., 1982] and consequently filament distribution. This relation is especially strong in July and August, in which months the years with most (fewest) filament occurrences were the ones with most (least) upwelling-favorable wind. Considering the relation between filament occurrences and northerly winds, at 40°N the WIM is separated into two distinct regions. Filaments mainly develop earlier and are more abundant in the southern region than in the northern region. The greater strength of northerly winds in the southern region lends support to the idea that upwelling-favorable wind is the main controlling factor in the development of filaments.

The number of filaments showed interannual variability, for example in the month of September filament occurrences ranged between 20 and 90. Regionally the interannual variability was greater in the northern sector, than in the south, and related to the variability of the wind. It was also evident that the number of filaments was more consistent between years in the peak months of filament production, July and August.

Results of modeling under climatological wind forcing indicated that, in some latitudes, the integrated filament distribution differed from the 10 year realistic simulation. As opposed to the interannual case, north of Vigo filaments rarely developed. This can be explained by the climatological wind field which is almost purely northerly, while real winds are mainly northeasterly or northwesterly. The former causes upwelling north of Cape Finisterre as reported by *Torres et al*. [2003]. Consequently upwelling in the neighborhood of Cape Finisterre is not well resolved, giving rise to a warmer temperature anomaly in the climatological simulation as discussed in *Nolasco et al*. [2013].

It is difficult to make a full quantitative analysis of the interaction of filaments with the eddy field because the location, size, strength, and sense of rotation of eddies all have a particular effect in individual eddy-filament relations. Nevertheless, the model simulation provided some examples of eddy-filament interactions in which the most important effects occurred during periods of wind relaxation when wind-driven currents are weaker, a situation that frequently occurs in late summer. The question of eddy-filament interactions deserves further dedicated investigation in this region.

In summary, a model simulation during a 10 year period was shown to be an efficient tool to study in a realistic way the filament field at the Western Iberian Margin. The main results of this study are:

1. Filament fields estimated with SST images, from the model and the satellite products, compare well with each other.
2. The results show that filament development was very similar to that described by *Haynes et al*. [1993] for a period of two decades earlier.
3. The preferential locations of filaments are associated with topographic irregularities (capes and promontories), or to instabilities likely associated with horizontal shear between equatorward upwelling flow and poleward flow offshore.
4. Latitude 40°N marks a separation between a northern filament region of weaker winds resulting in fewer filaments of variable position and oriented generally southwest, and a southern one of stronger upwelling-favorable winds, where filaments are more abundant, more anchored to coastal features, and slightly more southward.
5. Significant interannual variability in the number of filaments is observed throughout the upwelling season, but least in July and August, and is stronger in the northern region than the southern one.

6. A good representation of the wind field is important for retrieving realistic filament distributions, as shown by the failure of the climatological simulation to reproduce filaments in key regions where their presence is consistently observed.

Acknowledgments
This paper is a contribution to RAIA.co project (0520_RAIA_CO_1_E) funded by POCTEP and FEDER that supported NGF Cordeiro grant. A. Cordeiro-Pires was supported by the Portuguese Science and Technology Foundation (FCT) through PhD fellowship SFRH/BD/47500/2008. This work is part of the IMPROVE project, PTDC/MAR/110796/2009 funded by the FCT under the European Regional Development Fund. Satellite data used in this project can be obtained from http://www.osi-saf.org, other used data will be made available upon request to NGF Cordeiro (ngfc@ua.pt).

References

Antonov, J. I., D. Seidov, T. P. Boyer, R. A. Baranova, A. V. Mishonov, H. E. Garcia, O. K. Baranova, M. M. Zweng, and D. R. Johnson (2010), Volume 2: Salinity, *World Ocean Atlas 2009, NOAA Atlas NESDIS 69*, edited by S. Levitus, 184 pp., U.S. Gov. Print. Off., Washington, D. C.

Barth, J. A. (1994), Short-wave length instabilities on coastal jets and fronts, *J. Geophys. Res.*, *99*(C8), 16,095–16,115, doi:10.1029/94JC01270.

Bentamy, A., and D. C. Fillon (2011), Gridded surface wind fields from Metop/ASCAT measurements, *Int. J. Remote Sens.*, *33*, 1729–1754, doi:10.1080/01431161.2011.600348.

Bernstein, R. L., L. Breaker, and R. Whirtner (1977), California Current eddy formation: Ship, air and satellite results, *Science*, *195*, 353–359.

Breaker, L. C., and R. P. Gilliland (1981), A satellite sequence on upwelling along the California Coast, in *Coastal Upwelling*, edited by F. A. Richards, pp. 87–94, AGU, Washington, D. C., doi:10.1029/CO001p0087.

Cordeiro-Pires, A. (2013), Modeling the Western Iberian margin circulation: present and future, PhD thesis, Univ. de Aveiro, Aveiro, Portugal. [Available at http://ria.ua.pt/handle/10773/12191.]

Cravo, A., P. Relvas, S. Cardeira, F. Rita, M. Madureira, and R. Sánchez (2010), An upwelling filament off southwest Iberia: Effect on the chlorophyll a and nutrient export, *Cont. Shelf Res.*, *30*(15), 1601–1613.

da Silva, A. M., C. C. Young, and S. Levitus (1994), *Atlas of Surface Marine Data 1994, Vol. 1: Algorithms and Procedures. NOAA Atlas NESDIS 6*, 83 pp., U.S. Gov. Print. Off., Washington, D. C.

Fiúza, A. F. de G., M. E. de Macedo, and M. R. Guerreiro (1982), Climatological space and time variation of the Portuguese coastal upwelling, *Oceanol. Acta*, *5*, 31–40.

Flament, P., L. Armi, and L. Washburn (1985), The evolving structure of an upwelling filament, *J. Geophys. Res.*, *90*(C6), 11,765–11,778, doi:10.1029/JC090iC06p11765.

Graham, W. M., J. G. Field, and D. C. Potts (1992), Persistent "upwelling shadows" and their influence on zooplankton distributions, *Mar. Biol.*, *114*, 561–570.

Haynes, R., E. D. Barton, and I. Pilling (1993), Development, persistence, and variability of upwelling filaments off the Atlantic coast of the Iberian Peninsula, *J. Geophys. Res.*, *98*(C12), 22,681–22,692, doi:10.1029/93JC02016.

Ikeda, M., and W. J. Emery (1984), Satellite observations and modeling of meanders in the California Current System off Oregon and northern California, *J. Phys. Oceanogr.*, *14*, 1434–1450.

Kostianoy, A. G., and A. G. Zatsepin (1996), The West African coastal upwelling filaments and cross-frontal water exchange conditioned by them, *J. Mar. Syst.*, *7*, 349–359.

Locarnini, R. A., A. V. Mishonov, J. I. Antonov, T. P. Boyer, H. E. Garcia, O. K. Baranova, M. M. Zweng, and D. R. Johnson (2010), *Volume 1: Temperature, World Ocean Atlas 2009, NOAA Atlas NESDIS 68*, edited by S. Levitus, 184 pp., U.S. Gov. Print. Off., Washington, D. C.

M-F/CMS (2009), *North Atlantic Regional Sea Surface Temperature Product Manual*, vol. 1, 8th ed., Meteo-France, Lannion, France.

Marchesiello, P., J. C. McWilliams, and A. Shchepetkin (2003), Equilibrium structure and dynamics of the California Current System, *J. Phys. Oceanogr.*, *33*(4), 753–783.

Meunier, T., E. D. Barton, B. Barreiro, and B. Torres (2012), Upwelling filaments off Cap Blanc: Interaction of the NW African upwelling current and the Cape Verde frontal zone eddy field?, *J. Geophys. Res.*, *117*, C08031, doi:10.1029/2012JC007905.

Moita, M. T., P. B. Oliveira, J. C. Mendes, and A. S. Palma (2003), Distribution of chlorophyll *a* and *Gymnodinium catenatum* associated with coastal upwelling plumes off central Portugal, *Acta Oecol.*, *24*, S125–S132, doi:10.1016/S1146-609X(03)00011-0.

Narimousa, S., and T. Maxworthy (1989), Application of a laboratory model to the interpretation of satellite and field observations of coastal upwelling, *Dyn. Atmos. Oceans*, *13*(12), 1–46, doi:http://dx.doi.org/10.1016/0377-0265(89)90032-8.

Nencioli, F., C. Dong, T. D. Dickey, L. Washburn, and J. C. McWilliams (2010), A vector geometry based eddy detection algorithm and its application to a high-resolution numerical model product and high-frequency radar surface velocities in the Southern California Bight, *J. Atmos. Oceanic Technol.*, *27*(3), 564–579, doi:10.1175/2009JTECHO725.1.

Nolasco, R., A. Pires, N. Cordeiro, B. Cann, and J. Dubert (2013), A high-resolution modeling study of the Western Iberian Margin mean and seasonal upper ocean circulation, *Ocean Dyn.*, *63*(9–10), 1041–1062, doi:10.1007/s10236-013-0647-8.

Oliveira, P. B., R. Nolasco, J. Dubert, T. Moita, and A. Peliz (2009), Surface temperature, chlorophyll and advection patterns during a summer upwelling event off central Portugal, *Cont. Shelf Res.*, *29*(5–6), 759–774.

Peliz, A., T. L. Rosa, A. M. P. Santos, and J. L. Pissarra (2002), Fronts, jets, and counter-flows in the Western Iberian upwelling system, *J. Mar. Syst.*, *35*(1–2), 61–77.

Penven, P., L. Debreu, P. Marchesiello, and J. C. McWilliams (2006), Evaluation and application of the ROMS 1-way embedding procedure to the central California upwelling system, *Ocean Modell.*, *12*(1–2), 157–187, doi:10.1016/j.ocemod.2005.05.002.

Reboreda, R., N. G. F. Cordeiro, R. Nolasco, C. G. Castro, X. A. Álvarez-Salgado, H. Queiroga, and J. Dubert (2014), Modeling the seasonal and interannual variability (2001–2010) of chlorophyll-a in the Iberian margin, *J. Sea Res.*, *93*, 133–149.

Relvas, P., and E. D. Barton (2005), A separated jet and coastal counterflow during upwelling relaxation off Cape São Vicente (Iberian Peninsula), *Cont. Shelf Res.*, *25*(1), 29–49, doi:10.1016/j.csr.2004.09.006.

Relvas, P., E. D. Barton, J. Dubert, P. B. Oliveira, A. Peliz, J. C. B. da Silva, and A. M. P. Santos (2007), Physical oceanography of the western Iberia ecosystem: Latest views and challenges, *Prog. Oceanogr.*, *74*(2–3), 149–173.

Røed, L. P., and X. B. Shi (1999), A numerical study of the dynamics and energetics of cool filaments, jets, and eddies off the Iberian peninsula, *J. Geophys. Res.*, *104*(C12), 29,817–29,841, doi:10.1029/1999JC900175.

Serra, N., I. Ambar, and D. Boutov (2010), Surface expression of Mediterranean Water dipoles and their contribution to the shelf/slope-open ocean exchange, *Ocean Sci.*, *6*(1), 191–209.

Shchepetkin, A. F., and J. C. McWilliams (2005), The regional oceanic modeling system (ROMS): A split-explicit, free-surface, topography-following-coordinate oceanic model, *Ocean Modell.*, *9*(4), 347–404, doi:10.1016/j.ocemod.2004.08.002.

Strub, P. T., P. M. Kosro, and A. Huyer (1991), The nature of the cold filaments in the California Current System, *J. Geophys. Res.*, *96*(C8), 14,743–14,768, doi:10.1029/91JC01024.

Torres, R., E. D. Barton, P. Miller, and E. Fanjul (2003), Spatial patterns of wind and sea surface temperature in the Galician upwelling region, *J. Geophys. Res.*, *108*(C4), 3130, doi:10.1029/2002JC001361.

Troupin, C., E. Mason, J. M. Beckers, and P. Sagrá (2012), Generation of the Cape Ghir upwelling filament: A numerical study, *Ocean Modell.*, *41*, 1–15.

Veitch, J., P. Penven, and F. A. Shillington (2010), Modeling equilibrium dynamics of the Benguela Current System, *J. Phys. Oceanogr.*, *40*, 1942–1964.

Wooster, W. S., A. Bakun, and D. R. Mclain (1976), Seasonal upwelling cycle along the Eastern Boundary of the North-Atlantic, *J. Mar. Res.*, *34*(2), 131–141.